Supporting Information

Jha et al. 10.1073/pnas.1113874108

SI Text

Wild-type Δ^5-3-ketosteroid isomerase (KSI) from *Pseudomonas putida* contains three cysteine residues, which were mutated to serine to create a cysteine-free background for the preparation of single cysteine-containing mutant proteins. These mutations produce a negligible effect on catalysis (1). The enzymatic activity of one of the thiocyanate-labeled "D40" form of KSI (i.e., M116C-$^{13}C^{15}N$) has been measured in a previous work (2). The introduction of the thiocyanate probe results in only threefold reduction in enzyme activity, which is typical of the effects of mutation of the nonreacting, active site residues (3).

In this study, we have used four single cysteine-containing mutants of "D40N" form of KSI, in which the general base of the enzyme D40 has been mutated to N40. The D40N form of KSI mimics the charge distribution of the enzyme active site in the intermediate state (protonated base) (see main text) and is not the active form of the enzyme. All the four probe-modified proteins, however, bind coumarin 183 (C183) with similar affinity (legend to Fig. S1).

The four thiocyanate labeled D40N forms of KSI used in this study were named according to the position of the sole thiol group in the protein—i.e., M116C-$^{13}C^{15}N$, M105C-$^{13}C^{15}N$, F86C-$^{13}C^{15}N$, and I17C-$^{13}C^{15}N$. X-ray crystal structures of three of these probe-modified proteins (M116C-$^{13}C^{15}N$, M105C-$^{13}C^{15}N$, F86C-$^{13}C^{15}N$) with or without a bound intermediate analog equilenin have been determined in a previous study (4). The structure of I17C-$^{13}C^{15}N$ was modeled using PyMOL by placing thiocyanate in the space occupied by the isoleucine side chain in the crystal structure of KSI (Protein Data Bank ID 1OPY). The thiocyanate probes are located within a few angstroms of the polar, ionizable, and catalytic groups of the enzyme's active site.

Buffers. All the experiments were conducted in a pH 7.2, 40 mM potassium phosphate buffer containing 1 mM EDTA unless mentioned otherwise. Approximately 1% of DMSO was present in all the solutions containing C183.

Binding Experiments Using UV-Visible Absorption and Steady-State Fluorescence. UV-visible absorption spectra of free and enzyme-bound C183 were measured with a Perkin Elmer Lambda 25 spectrophotometer. The concentrations of C183 and KSI were, respectively, 5 and 50 μM. Steady-state fluorescence spectra of the unbound and enzyme-bound C183 were measured with a Perkin Elmer LS 55 fluorescence spectrometer, with excitation set to 408 nm. The binding constant of C183 to KSI was determined by monitoring the changes in the fluorescence emission spectra of C183 upon binding to KSI. The spectra were recorded keeping the concentration of C183 constant at 10 nM and varying the concentration of KSI from 0 to 10 μM.

Steady-State FTIR Experiments. All the steady-state IR-spectra were obtained on a Bruker Vertex 70 FTIR spectrometer equipped with an InSb detector. A band-pass (2,000–2,500 cm^{-1}) interference filter from Spectrogon was used. A gas-tight demountable liquid cell with sapphire windows and offset spacers (one 75-μm and one 100-μm spacer on either side) was used. Absorbance spectra were measured relative to a background taken with bovine serum albumin in water at equivalent concentration in grams per milliliter. Baselines were calculated using a polynomial fit (fourth to sixth order, depending on curvature) with roots defined at least 15 cm^{-1} distant from the peak maximum. Peak positions were determined using a second derivative-based method built into the OPUS FTIR software (Bruker Photonics).

C183 Binds to KSI in a Similar Manner as the Other Transition State Analogs. C183 when free in solution remains predominantly in its protonated form at pH 5 and exhibits an absorbance maximum at 355 nm (Fig. S1*A*). The deprotonated form of C183 absorbs maximally at 408 nm (Fig. S1*A*). The UV absorption maximum of C183 at pH 5 in the presence of KSI shifts from 355 to 408 nm, indicating that KSI binding converts C183 to its anionic form (Fig. S1*A*), as expected for a ligand with a solution pK_a of approximately 6.5 (5–7). The fluorescence emission of C183 ($\lambda_{max} = 450$ nm) is heavily quenched when it is bound to KSI (6) (Fig. S1*B*). A titration of the enzyme with varying amount of C183 was monitored by changes in fluorescence signal at 450 nm (Fig. S1 *B* and *C*) and the dissociation constant of KSI-C183 binding was determined to be approximately 1.3 μM (Fig. S1*C* and legend). C183 also contains a nitrile moiety at position 3 in its structure and the IR frequency of the nitrile also shifts upon binding, as expected for the formation of the anion.

KSI binds to many substituted phenols that serve as transition/intermediate-state analogs, with similar affinity (*ca.* 1–2 μM) (7). Many of these mimics of the enzyme–dienolate intermediate complex have been crystallized in previous studies, including KSI bound to the steroid equilenin, which like C183 is a naphthol derivative, and a number of substituted phenolates (7). KSI bound to phenolates and equilenin (whose solution pK_a is near to the KSI equiaffinity point and therefore binds as a mixture of protonated and deprotonated forms) (8) has been shown to have the same structure, within the resolution, as free KSI (7), and the bound phenolate ligand is superimposable on the A ring of equilenin (7). In both structures, the hydroxyl oxygen atom of the bound ligand is positioned to receive hydrogen bonds from oxyanion hole residues Tyr16 and Asp103. The binding interactions with the two distal rings of the substrate are known not to dictate the catalytic contributions from KSI's oxyanion hole (9), and hence it is not surprising that phenols, naphthols, and other intermediate analogs including C183 bind KSI with high affinity despite different number of aromatic rings in the structure and a variety of substituents.

Electronic Stark Experiments. The binding affinity of C183 to KSI was found to be greatly reduced in presence of the cryoprotectant (glycerol, sucrose, or trehalose) required for electronic Stark experiments, which are usually conducted at low temperature on frozen glasses (77 K). To mimic the protein-bound environment, the electronic Stark experiment was performed with C183 bound to (2-hydroxypropyl)-β-cyclodextrin. It is known that β-cyclodextrin binds to many fluorescent dyes including many classes of coumarin dyes due to its bucket-like structure (8). For electronic Stark experiments, 1 mM of C183 was mixed with 20 mM of (2-hydroxypropyl)-β-cyclodextrin in 1:1 pH 7.2 buffer/glycerol mixture, which forms a glass at 77 K. The solution (20 μL) was loaded into the sample cell and immediately plunged into liquid nitrogen. The sample cell consisted of two unpolished float glass slides coated with indium tin oxide ($R_s = 30$–60Ω , Delta Technologies), separated by approximately 50-μm thick Kapton spacers and mechanically held together with clips. Actual sample cell thicknesses were measured by recording the spectral interference fringes from 600 to 900 nm produced by the inner surfaces of the sample cell windows.

Electronic Stark experiments were performed on a custom-built setup as described previously (10). In brief, light from a mercury-xenon arc lamp was passed through a 0.22-m single monochromator, focused through the sample, and detected with a silicon photodiode. An ac field was supplied by a custom-built high-voltage power supply or a Trek Model 10/10 high-voltage power supply, which amplified an externally supplied, digitally generated sinusoidal voltage. Low-temperature spectra were taken in a liquid nitrogen immersion cryostat. The Stark signal (ΔI) was recorded with a lock-in amplifier (Stanford Research Systems SRS830) detecting at the second harmonic of the applied external field. The direct output voltage of the silicon photodiode (I) was recorded as well so that the change in absorption of the sample due to the externally applied field was calculated as $\Delta A = (\frac{2\sqrt{2}}{\ln 10})(\frac{\Delta I}{I})$. The Stark spectra were scaled to an electric field of 1 MV/cm. Absorption spectra were taken on the same setup. Absorption spectra fit well a single Gaussian equation. The Stark spectrum was analyzed as described previously (10–12). The Stark spectrum fit to a sum of first and second derivative of the absorption spectra of C183. Fig. S2 shows the electronic Stark spectra of C183. An analysis of the second derivative component of the fit, as described previously (10–12), yielded an electronic difference dipole of 14.2 debye. The value of local field correction factor, f, is taken as 1.2.

UV-Pump IR-Probe Experiments. We generated pump and probe pulses with a regeneratively amplified Ti:sapphire laser system (Spitfire, Spectra Physics) with a 1-kHz repetition rate and 35-fs FWHM pulse duration at 800 nm. We produced 400-nm pulses by frequency doubling the amplifier output with a 0.1-mm-thick beta barium borate crystal and sent approximately 5 mW to excite the electronic transition of C183. Tunable mid-IR pulses were generated by difference frequency generation of the near-IR signal and idler from an optical parametric amplifier (OPA800CF, Spectra Physics). These mid-IR pulses have a duration of 60 fs FWHM with spectral width of about 300 cm^{-1}. We dispersed the probe beam with a grating spectrometer (iHR320, Horiba Jobin Yvon) onto a liquid N_2-cooled 32×2 mercury-cadmium-telluride pixel array detector with a spectral resolution of approximately 1 cm^{-1} per pixel. The cross-correlation between the pump and probe is approximately 200 fs without further compression. The pump beam is intensity modulated pulse by pulse at 1 KHz by a mechanical chopper. As in conventional transient spectroscopy, we measure the difference absorption spectra between pump on and off:

$$S(\omega) = \frac{I_{\text{pump-on}}(\omega) - I_{\text{pump-off}}(\omega)}{I_{\text{pump-off}}(\omega)}. \qquad \textbf{[S1]}$$

The liquid samples were mounted between two CaF_2 windows with a 50-μm Teflon spacer. The sample cell was continuously rotated as well as vertically translated during the experiments to minimize photo damage of the samples. Transient spectra are averaged for approximately 5 h for each sample. Fig. S3 shows a representative transient infrared absorption contour plot for C116-$^{13}C^{15}N$.

The transient IR spectra were fitted to a sum of two pseudo-voigt functions to determine the nitrile stretching frequencies in the ground-state bleach and electronic excited state (Table 1). The exact value of the nitrile stretching frequencies depends upon the details of the lineshape function used to fit the data ($\Delta\tilde{\nu}_{CN}^{obs}$ differs by approximately ±25% depending upon the model used). However, stretching frequencies of the nitriles are time-independent irrespective of the model used to fit the data.

IR signals, $\Delta A_{\parallel}$ and $\Delta A_{\perp}$, when the polarizations of optical-pump and IR-probe beams are, respectively, parallel and perpendicular to each other, were monitored to calculate transient anisotropy and changes in angle, if any, between the nitrile-bond axis and optical transition dipole of C183. The anisotropy values in the electronic excited state appear to be slightly smaller than in the electronic ground state for all the three nitrile probes (Fig. 4 *A–C*, *Insets*). Although this difference in the anisotropy is at the border of the measurement accuracy, it could result from two different physical processes: (*i*) a change in orientation of the nitrile stretch transition dipole moment away from the C183 transition dipole moment, or (*ii*) a broadening of the distribution of relative orientations between the nitrile stretch transition dipole moment and the C183 transition dipole moment. The former reason is unlikely because any transient orientation of the nitrile group to the electric field induced by electronic excitation should increase the anisotropy, not decrease it. It would also lead to a time-dependent change in the nitrile stretch frequency, which we do not observe (Fig. 3). Hence, the more likely explanation of the decreased anisotropy in the electronic excited state is a subtle change in the thiocyano-group flexibility, rather than electrostatic alignment to the C183 excited state electric field. The broader orientational distribution would also provide an explanation for the comparatively wider line widths of the nitrile stretch in the electronic excited state than in the ground state.

Modeling of Vibrational Stark Shifts Observed in Visible-Pump IR-Probe Experiments. The photoexcitation of the enzyme-bound C183 is sensed by C116-$^{13}C^{15}N$, C86-$^{13}C^{15}N$, and C17-$^{13}C^{15}N$ as a vibrational Stark shift of 5, 4.2, and 4.1 cm^{-1}, respectively, to the red in their stretching frequency (Fig. 3 *A–C* and Table 1). The vibrational Stark shift experienced by C105-$^{13}C^{15}N$ was too small to measure reliably (Fig. 3*D*). A simple electrostatic model based upon the energy of a dipole in an electric field is used to estimate the vibrational Stark shifts ($\Delta\tilde{\nu}_{CN}$) experienced by C116-$^{13}C^{15}N$, C86-$^{13}C^{15}N$, C17-$^{13}C^{15}N$, and C105-$^{13}C^{15}N$ dipoles, due to the change in electrostatic environment caused by photoexcitation of C183. The electric field $\Delta\vec{F}$ created by the electronic difference dipole of C183 (positioned along the z axis) at the location of a nitrile probe as shown in Fig. S4 would be given in a spherical coordinate system by

$$\Delta\vec{F} = \frac{|\Delta\vec{\mu}_{\text{excitation}}|}{4\pi\varepsilon_R\varepsilon_0 r^3}(2\cos\theta\hat{r} + \sin\theta\hat{\theta}), \qquad \textbf{[S2]}$$

$$|\Delta\vec{F}_r| = \frac{2|\Delta\vec{\mu}_{\text{excitation}}|\cos\theta}{4\pi\varepsilon_R\varepsilon_0 r^3}, \qquad \textbf{[S2a]}$$

$$|\Delta\vec{F}_\theta| = \frac{|\Delta\vec{\mu}_{\text{excitation}}|\sin\theta}{4\pi\varepsilon_R\varepsilon_0 r^3}, \qquad \textbf{[S2b]}$$

where $\Delta\vec{F}_r$ and $\Delta\vec{F}_\theta$ are components of the electric field, $\Delta\vec{F}$, along the direction of unit vector $\hat{r}$ and $\hat{\theta}$, respectively; r is the distance from the center of the electronic difference dipole to the center of the nitrile bond, $\hat{r}$ is the unit vector in the direction of r, θ is the angle between the z axis and the displacement vector $\vec{r}$, $\hat{\theta}$ is the unit vector perpendicular to vector $\hat{r}$, $|\Delta\vec{\mu}_{\text{excitation}}|$ is the magnitude of the electronic difference dipole of C183, ε_0 is the permittivity of vacuum, and ε_R is the relative permittivity of the protein medium.

The magnitude of the change in electric field, $\Delta\vec{F}$, projected along the difference dipole of the nitrile ($\Delta\vec{\mu}_{CN}$) (which aligns with the nitrile-bond axis), is given by

$$|\Delta\vec{F}| = |\Delta\vec{F}_r|\cos\alpha + |\Delta\vec{F}_\theta|\cos\beta, \qquad \textbf{[S3]}$$

where α and β are the respective angles that $\Delta\vec{F}_r$ and $\Delta\vec{F}_\theta$ make with $\Delta\vec{\mu}_{CN}$ (Fig. S4). Because $\Delta\vec{F}$ and $\Delta\vec{\mu}_{CN}$ are in the same direction (parallel to the −CN bond axis), $\Delta\tilde{\nu}_{CN}$ could be estimated using Eq. **1** (see manuscript text),

$$\Delta\tilde{\nu}_{CN} = \frac{|\Delta\vec{F}||\Delta\vec{\mu}_{CN}|}{hc}. \quad [S4]$$

The magnitude of $\Delta\vec{\mu}_{CN}$ is 0.7 $cm^{-1}/(MV/cm)$ (11). Table S2 lists the values of θ, r, α, and β for C116-$^{13}C^{15}N$, C86-$^{13}C^{15}N$, C17-$^{13}C^{15}N$, and C105-$^{13}C^{15}N$ probe dipoles measured using the structural model of KSI bound to C183 shown in Fig. 1.

In this simple model, it is assumed that (*i*) the changes in the charge distribution due to the movement of electronic charges as a result of photoexcitation of C183 can be approximated by its electronic difference dipole, and (*ii*) the electronic difference dipole of C183 lies in the direction of the optical transition dipole. The direction of the optical transition dipole of C183 was estimated by measuring the difference IR spectra of the nitrile attached to C183 when the polarization of the IR-probe beam is parallel and perpendicular to the optical-pump beam (using Eq. **2**, see main manuscript). Fig. S6 shows that the optical transition dipole of C183 makes an angle of approximately 30° (legend to Fig. S6) with the IR-transition dipole of the nitrile (attached to C183), which aligns with the axis of the nitrile bond. This measurement is in line with a previous report that the optical transition dipoles of coumarins lie roughly along the long axis of the molecule (13).

The value of $\Delta\tilde{\nu}_{CN}$ predicted from the model is dependent upon the value of ε_R (Table S2). It is remarkable, however, that this simple model predicts the experimentally observed shifts in vibrational frequency of nitriles (in response to the photoexcitation of C183) so well by varying the value of ε_R between just 1 and 2. The value of $\Delta\tilde{\nu}_{CN}$ predicted from the model match the experimentally observed vibrational Stark shift ($\Delta\tilde{\nu}_{CN}^{obs}$), in both sign and magnitude, by taking a value of $\varepsilon_R \sim 1.5$ in case of C116-$^{13}C^{15}N$; $\varepsilon_R \sim 1.0$ in case of C86-$^{13}C^{15}N$; and $\varepsilon_R \sim 2.0$ in case of C17-$^{13}C^{15}N$. Note that the spectator probes are close to the chromophore so one would not expect appreciable dielectric screening. It is important to note that the structural model presented in Fig. 1*A* combined with the simple electrostatic model discussed above also explains the reduced sensitivity of C105-$^{13}C^{15}N$ because this nitrile probe is nearly perpendicular to the C183 ring (Table S2). The close correspondence between the calculated ($\Delta\tilde{\nu}_{CN}$) (Table S2) and experimentally observed ($\Delta\tilde{\nu}_{CN}^{obs}$) (Table 1) values of vibrational Stark shifts also indicates that the structural model presented in Fig. 1*A* and assumptions made in the model above are reasonable. One of the advantages of the simple electrostatic model used here is that it avoids the estimation of charge distributions in the electronic excited state of the dye (14, 15).

1. Kim SW, et al. (1997) Mutational analysis of the three cysteines and active-site aspartic acid 103 of ketosteroid isomerase from Pseudomonas putida biotype B. *J Bacteriol* 179:7742–7747.
2. Sigala PA, Fafarman AT, Bogard PE, Boxer SG, Herschlag D (2007) Do ligand binding and solvent exclusion alter the electrostatic character within the oxyanion hole of an enzymatic active site? *J Am Chem Soc* 129:12104–12105.
3. Axe DD, Foster NW, Fersht AR (1998) A search for single substitutions that eliminate enzymatic function in a bacterial ribonuclease. *Biochemistry* 37:7157–7166.
4. Fafarman AT, Sigala PA, Herschlag D, Boxer SG (2010) Decomposition of vibrational shifts of nitriles into electrostatic and hydrogen-bonding effects. *J Am Chem Soc* 132:12811–12813.
5. Childs W, Boxer SG (2010) Proton affinity of the oxyanion hole in the active site of ketosteroid isomerase. *Biochemistry* 49:2725–2731.
6. Childs W, Boxer SG (2010) Solvation response along the reaction coordinate in the active site of ketosteroid isomerase. *J Am Chem Soc* 132:6474–6480.
7. Kraut DA, et al. (2006) Testing electrostatic complementarity in enzyme catalysis: Hydrogen bonding in the ketosteroid isomerase oxyanion hole. *PLoS Biol* 4:e99.
8. Hansen PE, Dettman HD, Heather DD, Sykes BD (1985) Solvent-induced deuterium isotope effects on ^{19}F chemical shifts of some substituted fluorobenzenes. Formation of incusion complexes. *J Magn Reson* 62:487–496.
9. Schwans JP, Kraut DA, Herschlag D (2009) Determining the catalytic role of remote substrate binding interactions in ketosteroid isomerase. *Proc Natl Acad Sci USA* 106:14271–14275.
10. Silverman LN, Spry DB, Boxer SG, Fayer MD (2008) Charge transfer in photoacids observed by stark spectroscopy. *J Phys Chem A* 112:10244–10249.
11. Andrews SS, Boxer SG (2000) Vibrational stark effects of nitriles I. Methods and experimental results. *J Phys Chem A* 104:11853–11863.
12. Bublitz GU, Boxer SG (1997) Stark spectroscopy: applications in chemistry, biology, and materials science. *Annu Rev Phys Chem* 48:213–242.
13. Wang C, Akhremitchev B, Walker GC (1997) Femtosecond infrared and visible spectroscopy of photoinduced intermolecular electron transfer dynamics and solvent-solute reaction geometries: Coumarin 337 in dimethylaniline. *J Phys Chem A* 101:2735–2738.
14. Mente SR, Maroncelli M (1999) Computer simulations of the solvatochromism of betaine-30. *J Phys Chem B* 103:7704–7719.
15. Baiz CR, Kubarych KJ (2010) Ultrafast vibrational Stark-effect spectroscopy: Exploring charge-transfer reactions by directly monitoring the solvation shell response. *J Am Chem Soc* 132:12784–12785.

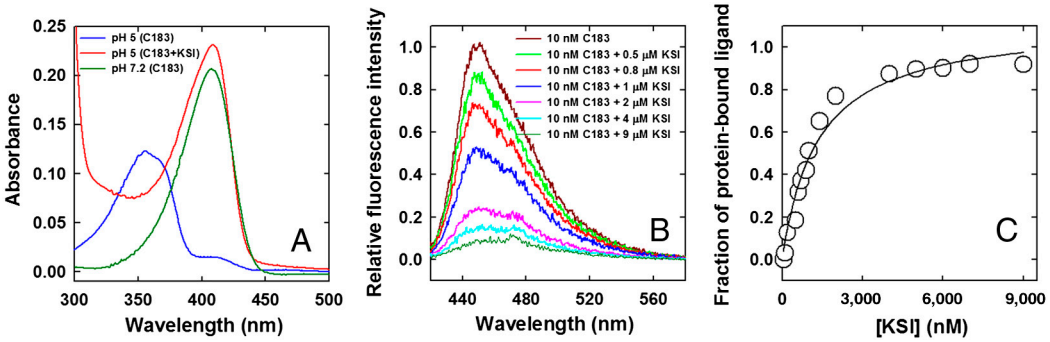

Fig. S1. C183 binds tightly to KSI in anionic form. (*A*) Absorption spectra of C183 when it is free in solution at pH 5 (blue line) and pH 7.2 (green line). The red line shows the absorption spectra of C183 at pH 5 in presence of M116C-$^{13}C^{15}N$ variant of KSI-D40N. *B* shows the decrease in fluorescence emission intensity of C183 when it is bound to M116C-$^{13}C^{15}N$. In *C*, the fraction of protein-bound C183 is plotted against the total protein concentration (circles) and a fit of the data to the equation ($y = \frac{B_{max}x}{K_d+x}$) yields a value of $K_d = 1.3$ μM. All the four probe-modified proteins, M116C-$^{13}C^{15}N$, F86C-$^{13}C^{15}N$, I17C-$^{13}C^{15}N$, and M105C-$^{13}C^{15}N$ bind C183 with similar affinity and the measured values of K_d are similar (1.2 ± 0.2 μM).

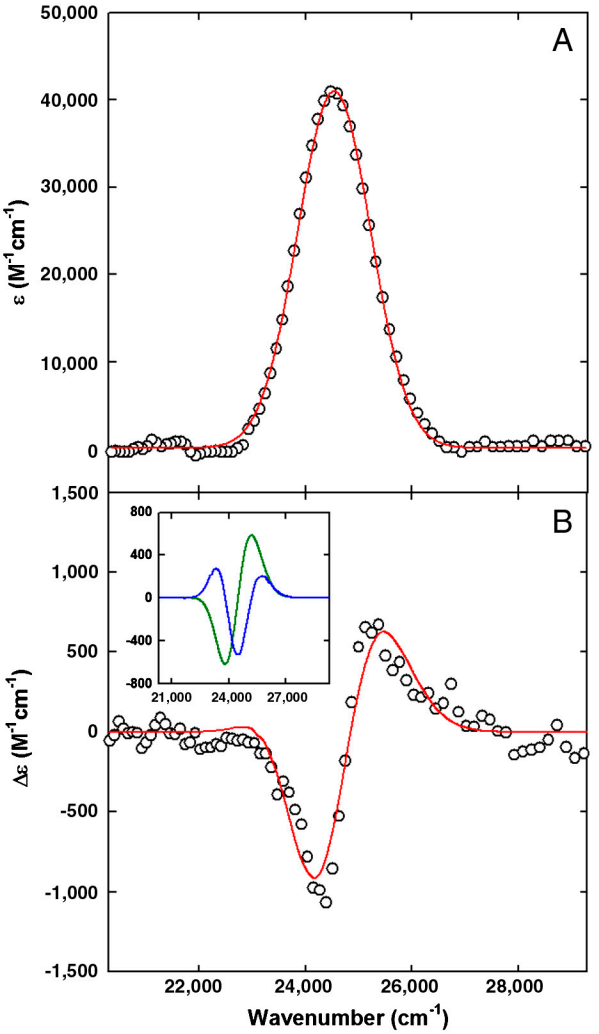

Fig. S2. Absorption and Stark spectra of C183 bound to (2-hydroxypropyl)-β-cyclodextrin. (*A*) Absorption spectra at 77 K (circles) fitted to a Gaussian equation (red line). (*B*) Stark spectra (circles) and fit of the Stark spectra to a sum of first and second derivatives of the absorption spectra (red line). *B* (*Inset*) shows the first (green line) and the second (blue line) derivative components of the fit. The second derivative component of the fit yields an electronic difference dipole of 14.2 debye (10).

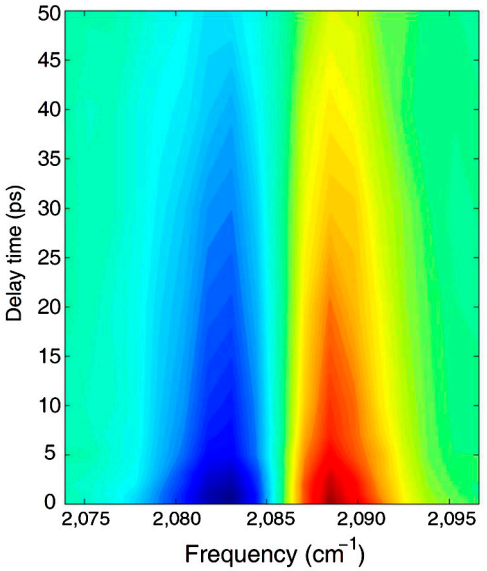

Fig. S3. Temporally and spectrally resolved transient UV-pump–IR-probe data for C116C-$^{13}C^{15}N$. The transient spectra represent the vibrational stark shift of nitrile stretch induced by photoexcitation of C183. The temporal behavior clearly indicates the static vibrational frequencies in both the electronic ground and excited states.

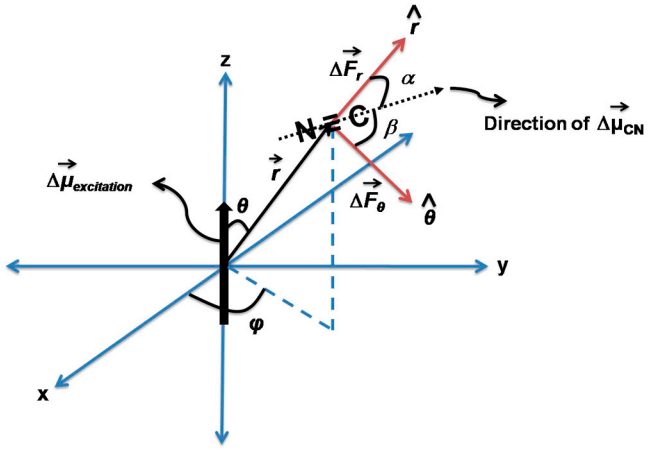

Fig. S4. Modeling of vibrational Stark shift. The electronic difference dipole of C183 is positioned along the *z* axis and the electric field experienced by enzyme-bound nitriles due to the electronic difference dipole of C183 was calculated using Eqs. **S2**–**S4**. The values of *r*, θ, α, and β for the four enzyme-bound nitrile probes C116-$^{13}C^{15}N$, C86-$^{13}C^{15}N$, C17-$^{13}C^{15}N$, and C105-$^{13}C^{15}N$ are determined from the structural model presented in Fig. 1*A* by using the program PyMOL, and are listed in Table S2.

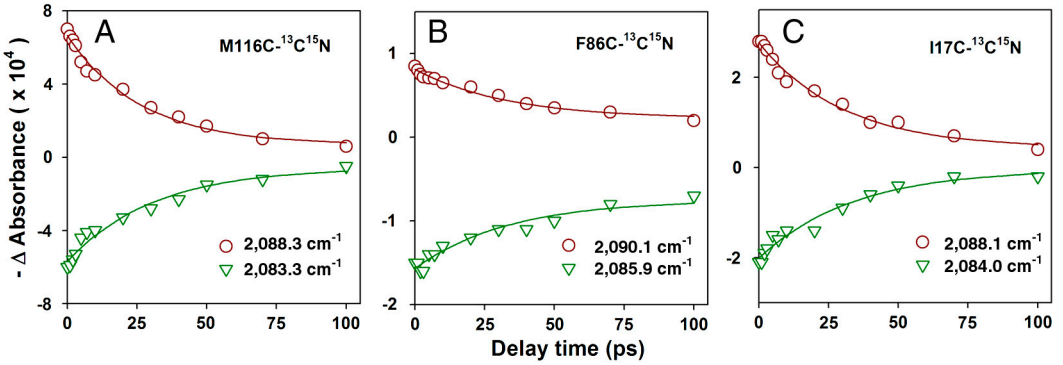

Fig. S5. Kinetics of change in transient IR signal intensity of the nitrile stretch in the electronic ground state bleach (dark-red circles) and the electronic excited state (inverted green triangles) of KSI-bound C183. (*A*) M116C-$^{13}C^{15}N$; (*B*) F86C-$^{13}C^{15}N$; (*C*) I17C-$^{13}C^{15}N$. In each panel, the solid line through the data is a fit to a single exponential equation. The transient IR signals, in both ground-state bleach and electronic excited states, change with a similar time constant (31 $\pm$ 3 ps) for all the three proteins.

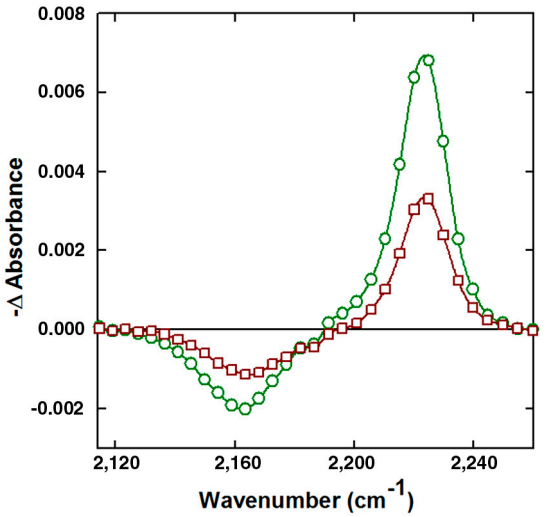

Fig. S6. Transient difference IR-absorption spectra of nitrile attached to enzyme-bound C183 after the photoexcitation of C183 at 400 nm when the polarization of pump and probe beams are parallel (green circles) and perpendicular (dark-red squares) to each other. An analysis of the $\Delta A_{\parallel}$ and $\Delta A_{\perp}$ signals at 2,166.1 cm^{-1} using Eq. **2** yields a value of anisotropy of approximately 0.25, which corresponds to an average angle of approximately 30° between the optical transition dipole of C183 and IR-transition dipole of nitrile of C183.

Table S1. Mean vibrational frequencies for nitrile-modified KSI-D40N at pH 7.2

	$\bar{\nu}_{CN}$ (FWHM), cm^{-1}		
	Apo form		
Probe location	Major peak	Minor peak	C183 bounded form
C116-$^{13}C^{15}N$*	2,084.2 (7.5)	—	2,088.5 (9)
C86-$^{13}C^{15}N$	2,090.4 (5.4)	2,084.6 (6.8)	2,090.2 (11.4)
C17-$^{13}C^{15}N$	2,083.9 (7.8)	2,091.9 (4.1)	2,088.1 (8.9)
C105-$^{13}C^{15}N$*	2,076.1 (3.5)	—	2,075.8 (4.7)

*The apo form of C116-$^{13}C^{15}N$ and C105-$^{13}C^{15}N$ have unimodal vibrational spectra.

Table S2. Modeling of vibrational Stark shifts

Parameters	C116-$^{13}C^{15}N$	C86-$^{13}C^{15}N$	C17-$^{13}C^{15}N$	C105-$^{13}C^{15}N$*
r, Å	6.5	6.3	7.5	10.6
θ, °	36	48	45	7
α, °	46	106	0	97
β, °	136	16	90	187
$\Delta\bar{\nu}_{CN}$ ($\varepsilon_R = 1$),† cm^{-1}	−7.6	−4.1	−9	+0.77
$\Delta\bar{\nu}_{CN}$ ($\varepsilon_R = 2$),† cm^{-1}	−3.8	−2.07	−4.5	+0.4
$\Delta\bar{\nu}_{CN}^{obs}$,‡ cm^{-1}	−5	−4.2	−4.1	—

The values of various parameters in Eqs. **S2**–**S4**, determined using PyMOL for all four vibrational spectator probes.

*The direction of Stark shift (blue versus red) is highly dependent on error in the angle θ as the −CN dipole is nearly perpendicular to $\vec{r}$.

†For calculation of $\Delta\bar{\nu}_{CN}$, the value of $|\Delta\vec{\mu}_{excitation}|$ and ε_0 in Eqs. **S2a** and **S2b** is taken as 4.69×10^{-29} C · m (14.2 debye) and 8.85×10^{-12} F · m^{-1}, respectively.

‡$\Delta\bar{\nu}_{CN}^{obs}$ are the experimentally observed Stark shifts and the values are taken from Table 1.